

High-Gain Disturbance Observer for Robust Trajectory Tracking of Quadrotors

Mohammadreza Izadi¹ and Reza Faieghi*¹

¹Department of Aerospace Engineering, Toronto Metropolitan University, Toronto, Canada

Abstract

This paper presents a simple method to boost the robustness of quadrotors in trajectory tracking. The presented method features a high-gain disturbance observer (HGDO) that provides disturbance estimates in real-time. The estimates are then used in a trajectory control law to compensate for disturbance effects. We present theoretical convergence results showing that the proposed HGDO can quickly converge to an adjustable neighborhood of actual disturbance values. We will then integrate the disturbance estimates with a typical robust trajectory controller, namely sliding mode control (SMC), and present Lyapunov stability analysis to establish the boundedness of trajectory tracking errors. However, our stability analysis can be easily extended to other Lyapunov-based controllers to develop different HGDO-based controllers with formal stability guarantees. We evaluate the proposed HGDO-based control method using both simulation and laboratory experiments in various scenarios and in the presence of external disturbances. Our results indicate that the addition of HGDO to a quadrotor trajectory controller can significantly improve the accuracy and precision of trajectory tracking in the presence of external disturbances.

Keywords: high gain observer, disturbance observer, nonlinear control, sliding mode control

1 Introduction

Recently, quadrotor uncrewed aerial vehicles (UAVs) have garnered significant attention from researchers due to their potential applications, including tasks like power line monitoring, inspection, logistics distribution, and firefighting. To execute these complex missions accurately and with high quality, it is crucial to ensure the stability and robustness of the position and attitude control systems. However, achieving robustness is a challenging task when dealing with external disturbances. Quadrotors are susceptible to various external disturbances, including wind gusts [1], airflow distortion in the vicinity of surfaces [2], and wake turbulence [3]. These disturbances are often unmodeled or challenging to measure. Consequently, enhancing reliability and safety in trajectory-tracking missions has emerged as a formidable challenge.

*Corresponding author: reza.faieghi@torontomu.ca

Various control approaches are studied for robust trajectory tracking of vehicles in the presence of disturbances. Examples include model predictive control [4, 5, 6], sliding mode control (SMC) [7, 8, 9, 10], adaptive control [11, 12], neural networks [13], and reinforcement learning [14].

Numerous control methods exist that rely on disturbance observers (DOs). For example, the time delay controller (TDC) involves a DO that uses the time delay between the control input and the system output to estimate the disturbance [15], successfully applied to quadrotor attitude control, altitude control, and position control [16]. Sliding mode DO is another variation of DOs that relies on a sliding mode observer to estimate the disturbance, improving the vehicle robustness to external disturbances and sensor noise [17]. Further examples include generalized extended state observer [18], and the uncertainty and disturbance estimator (UDE) [19, 20]. The latter offers several advantages, including the absence of system delays, the elimination of control signal oscillations, and the obviation of the need to measure state vector derivatives [21].

The challenge of disturbances in constrained systems has been addressed by using iterative learning control, taking into account both input and output constraints, along with model uncertainty and output disturbances [22]. The use of DO in a hierarchical control framework combined with adaptive control techniques is investigated in [23], enabling quadrotors to adapt to varying disturbances and compensate for aerodynamic damping effects, resulting in robust and precise control. A bank of nonlinear DOs is utilized alongside a set of generalized backstepping and SMCs to counteract the impact of unaccounted uncertainties that affect the vehicle during flight [24]. Finite-time nonlinear DO is studied in [25]. An integrated adaptive dynamic programming (ADP) technique is used in [26] to achieve asymptotic tracking. By using real-time input-output data, the control algorithm can compute an approximated optimal fault-tolerant control. This approach allows the system to reject disturbances and maintain stable performance even in the presence of uncertainties and faults.

While DO-based control is proven to be effective for quadrotor trajectory tracking, many existing DOs suffer from complex structures that add to the computational overhead of flight controllers. While significant progress has been made on the computational power of flight controllers, the extensive computational demands for autonomous or semi-autonomous operations, coupled with the power and weight restrictions of quadrotors, impose constraints on the available computing power of flight controllers; therefore, simple and computationally efficient DOs are still desired. Also, complex DOs often involve several tuning parameters which require an involved tuning process to ensure a fast convergence rate.

One category of nonlinear observers that are simple and fast is high-gain observers (HGOs) [27]. As its name suggests, HGO relies on the idea of applying a high gain to quickly recover the state estimates. HGOs present several desirable properties. First, they are relatively simple to design and implement since the observer is a copy of the model of the system with a gain whose expression is explicitly given. Second, the observer tuning is realized simply through the choice of a single scalar design parameter. Finally, they can provide global or semi-global stability results for a large class of systems. Such appealing properties; however, come at a cost. Conventional HGOs suffer from measurement noise amplification; however, this problem is alleviated by recent designs [28, 29].

Given the advantages of HGOs, their applications for disturbance estimation are also explored, giving rise to high-gain disturbance observers (HGDOs) [30]. However, it has not been thoroughly studied for quadrotors, especially on an actual vehicle with real measurement

errors and real disturbances, beyond simulation. The papers that we were able to find on this topic either presented a limited simulation study or focused on only attitude control [31, 32, 33, 18]. Another related work is [34] which does not design HGDO, but rather an HGO for quadrotor state estimation, as an alternative to the extended Kalman filter. It is worth noting that the application of HGDOs for helicopters has been studied in a few research papers [35, 36]. While helicopters and quadrotors are both rotary-wing aircraft, there exist fundamental differences in their flight mechanisms and control. Moreover, the tail rotor in helicopters adds an additional degree of authority for lateral control, which is missing in quadrotors.

In light of the above discussion, our objective here is to design HGDO for trajectory control of quadrotors. The main contribution of this paper is that it develops HGDO for the attitude and position control of quadrotors. We integrated the proposed HGDO with a Lyapunov-based robust control law, namely SMC. We conduct extensive simulation and hardware experiments to compare the proposed HGDO+SMC method with existing methods. Our results demonstrate fast and accurate disturbance estimation, enabling accurate trajectory tracking for quadrotors, outperforming the benchmark methods tested. We present Lyapunov stability analysis to establish the boundedness of tracking errors and disturbance estimations. The SMC can be easily replaced by another Lyapunov-based controller, and a similar stability analysis can be derived for the alternative controller. Overall, our intention is not a major overhaul in the quadrotor flight control, but rather to introduce a simple, easy-to-tune, and computationally efficient module that can be added to a flight controller and boost trajectory tracking robustness against external disturbances.

2 Quadrotor Modeling

The details of the quadrotor model are explained in various references such as [37]. Here, we attempt to write the quadrotor translation and rotational dynamics in second-order controllability canonical forms which will become useful in our developments. The problem statement will follow.

Let us begin by setting $\mathcal{I} = \{\mathbf{x}_{\mathcal{I}}, \mathbf{y}_{\mathcal{I}}, \mathbf{z}_{\mathcal{I}}\}$ as an Earth-fixed inertial coordinates frame, and $\mathcal{B} = \{\mathbf{x}_{\mathcal{B}}, \mathbf{y}_{\mathcal{B}}, \mathbf{z}_{\mathcal{B}}\}$ as the body-fixed coordinates frame whose origin coincides with the center of mass of the vehicle (Fig. 1). We assume that the quadrotor body is rigid and symmetric, with arms aligned to $\mathbf{x}_{\mathcal{B}}$ and $\mathbf{y}_{\mathcal{B}}$. The length of each arm is l , and the mass of the vehicle is m . Also, the inertia matrix is \mathbf{J} which is diagonal $\mathbf{J} = \text{diag}(J_x, J_y, J_z)$ due to the symmetry of the vehicle.

We denote the position of the vehicle in \mathcal{I} by $\boldsymbol{\xi} = [x, y, z]^T$. For the vehicle attitude, we use $\boldsymbol{\eta} = [\phi, \theta, \psi]^T$, where $-\pi < \phi \leq \pi$, $-\frac{\pi}{2} \leq \theta \leq \frac{\pi}{2}$, and $-\pi < \psi \leq \pi$ are the Euler angles representing pitch, roll, and yaw in the yaw-pitch-roll sequence. With the above Euler angle configuration, the rotation matrix from \mathcal{B} to \mathcal{I} takes the following form

$$\mathbf{R} = \begin{bmatrix} c\theta c\psi & s\phi s\theta c\psi - c\phi s\psi & c\phi s\theta c\psi + s\phi s\psi \\ c\theta s\psi & s\phi s\theta s\psi + c\phi c\psi & c\phi s\theta s\psi - s\phi c\psi \\ -s\theta & s\phi c\theta & c\phi c\theta \end{bmatrix}, \quad (1)$$

where c and s stand for cosine and sine functions. Also, if $\boldsymbol{\omega} = [p, q, r]^T$ represents the angular velocity vector, then according to the Euler kinematical equation, we have $\dot{\boldsymbol{\eta}} = \mathbf{H}(\boldsymbol{\eta}) \boldsymbol{\omega}^{\mathcal{B}}$,

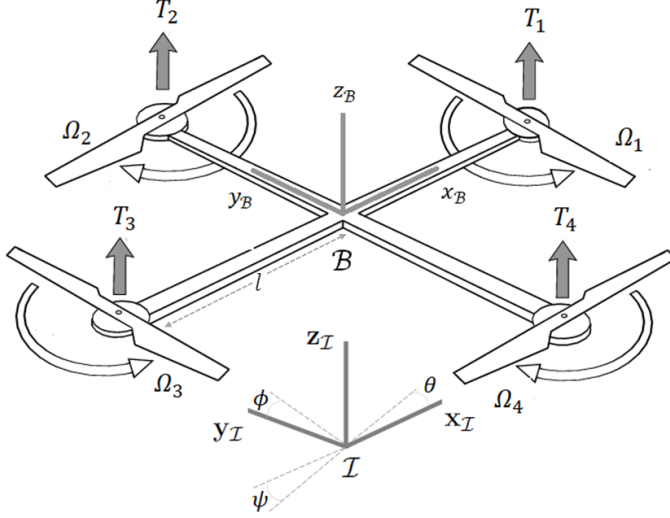


Figure 1: Quadrotor model and coordinate frames

where the superscript \mathcal{B} indicates that the vector components are expressed in \mathcal{B} and

$$\mathbf{H}(\boldsymbol{\eta}) = \begin{bmatrix} 1 & \sin \phi \tan \theta & \cos \phi \tan \theta \\ 0 & \cos \phi & -\sin \phi \\ 0 & \sin \phi / \cos \theta & \cos \phi / \cos \theta \end{bmatrix}. \quad (2)$$

Each of the vehicle's rotors produces a thrust T_i , $i = \{1, 2, 3, 4\}$ in the direction of \mathbf{z}_B . T_i s are usually approximated by $k_T \Omega_i^2$ where Ω_i is the angular velocity of i -th rotor, and k_T is a coefficient. The rotor angular velocities on the \mathbf{x}_B and \mathbf{y}_B axes have opposite signs ($\Omega_{1,3} > 0$, $\Omega_{2,4} < 0$) to counterbalance the reaction torque induced by the rotors and to control ψ . Let \mathbf{f}_A and $\boldsymbol{\tau}_A$ be the aerodynamic force and torque vectors produced by T_i s. Then, we can express them in \mathcal{B} as follows

$$\mathbf{f}_A^{\mathcal{B}} = \begin{bmatrix} 0 \\ 0 \\ T \end{bmatrix}, \text{ and } \boldsymbol{\tau}_A^{\mathcal{B}} = \begin{bmatrix} lk_T (\Omega_4^2 - \Omega_2^2) \\ lk_T (\Omega_3^2 - \Omega_1^2) \\ lk_Q (\Omega_1^2 - \Omega_2^2 + \Omega_3^2 - \Omega_4^2) \end{bmatrix}, \quad (3)$$

where l is the distance from the center of mass to the rotor, $T = k_T \sum_{i=1}^4 \Omega_i^2$ is the total thrust, k_T is thrust coefficient and k_Q is torque coefficient. The efficiency of the propulsion system is greatly affected by the thrust and torque coefficients, which are shaped by the rotor's design characteristics. These coefficients are also affected by the motion of the vehicle as detailed in [38, 39].

In addition, we assume that there exist two unknown disturbance vectors $\mathbf{d}_\xi = [d_x, d_y, d_z]^T$ and $\mathbf{d}_\eta = [d_\phi, d_\theta, d_\psi]^T$.

Applying Newton's law of motion, the translational dynamics of the vehicle take the following form

$$\ddot{\boldsymbol{\xi}} = -\mathbf{g} + \frac{1}{m} (\mathbf{f}_A^{\mathcal{I}} + \mathbf{d}_\xi^{\mathcal{I}}), \quad (4)$$

where $\mathbf{f}_A^{\mathcal{I}} = \mathbf{R}\mathbf{f}_A^{\mathcal{B}}$, $\mathbf{d}_\xi^{\mathcal{I}} = \mathbf{R}\mathbf{d}_\xi^{\mathcal{B}}$ and $\mathbf{g} = [0 \ 0 \ g]^T$ is the gravity vector with g set to $9.81m/s^2$. Using Euler's rotation theorem, the rotational dynamics of the vehicle take the following

form

$$\dot{\boldsymbol{\omega}}^{\mathcal{B}} = \mathbf{J}^{-1} (-\boldsymbol{\omega}^{\mathcal{B}} \times \mathbf{J}\boldsymbol{\omega}^{\mathcal{B}} + \boldsymbol{\tau}_A^{\mathcal{B}} + \mathbf{d}_{\xi}^{\mathcal{B}}), \text{ and } \dot{\boldsymbol{\eta}} = \mathbf{H}(\boldsymbol{\eta}) \boldsymbol{\omega}^{\mathcal{B}}, \quad (5)$$

where the index \times indicates the cross product.

We can now use (4) and (5) to write the quadrotor dynamics as a set of second-order nonlinear systems in controllability canonical forms. However, due to the particular structure of (5), the equations will become complicated, and this will lead to complex DO and control laws. If ϕ and θ are small, \mathbf{H} can be greatly simplified such that $\dot{\boldsymbol{\eta}} \approx \boldsymbol{\omega}$. As such, the expressions in (4) and (5) transfer into

$$\begin{cases} \ddot{x} = (\cos \varphi \sin \theta \cos \psi + \sin \varphi \sin \psi) \frac{1}{m} u_1 + d_x, \\ \ddot{y} = (\cos \varphi \sin \theta \sin \psi - \sin \varphi \sin \psi) \frac{1}{m} u_1 + d_y, \\ \ddot{z} = -g + (\cos \varphi \cos \theta) \frac{1}{m} u_1 + d_z, \\ \ddot{\phi} = \dot{\theta} \dot{\psi} \left(\frac{I_y - I_z}{I_x} \right) + \frac{1}{I_x} u_2 + d_{\phi}, \\ \ddot{\theta} = \dot{\varphi} \dot{\psi} \left(\frac{I_z - I_x}{I_y} \right) + \frac{1}{I_y} u_3 + d_{\theta}, \\ \ddot{\psi} = \dot{\varphi} \dot{\theta} \left(\frac{I_x - I_y}{I_z} \right) + \frac{1}{I_z} u_4 + d_{\psi}. \end{cases} \quad (6)$$

By setting $\mathbf{x}_1 = \boldsymbol{\xi}$, $\mathbf{x}_2 = \dot{\boldsymbol{\xi}}$, $\mathbf{x}_3 = \boldsymbol{\eta}$, $\mathbf{x}_4 = \dot{\boldsymbol{\eta}}$, $\mathbf{d}_1 = \frac{\mathbf{d}_{\xi}}{m}$, $\mathbf{d}_2 = \mathbf{J}^{-1} \mathbf{d}_{\eta}$, $\mathbf{u}_1 = \frac{1}{m} \mathbf{b} u_1$, $\mathbf{u}_2 = [u_2/I_x, u_3/I_y, u_4/I_z]^T$, $\mathbf{g} = [0, 0, g]^T$,

$$\mathbf{b} = \begin{bmatrix} c\varphi s\theta c\psi + s\varphi s\psi \\ c\varphi s\theta s\psi - s\varphi c\psi \\ c\varphi c\theta \end{bmatrix}, \text{ and } \mathbf{f}_2(\mathbf{x}_4) = \begin{bmatrix} \frac{J_y - J_z}{J_x} \dot{\theta} \dot{\psi} \\ \frac{J_z - J_x}{J_y} \dot{\phi} \dot{\psi} \\ \frac{J_x - J_y}{J_z} \dot{\phi} \dot{\theta} \end{bmatrix},$$

the equations in (6) can be converted into the following state space representation

$$\begin{cases} \dot{\mathbf{x}}_1 = \mathbf{x}_2, \\ \dot{\mathbf{x}}_2 = -\mathbf{g} + \mathbf{u}_1 + \mathbf{d}_1, \\ \dot{\mathbf{x}}_3 = \mathbf{x}_4, \\ \dot{\mathbf{x}}_4 = \mathbf{f}_2(\mathbf{x}_4) + \mathbf{u}_2 + \mathbf{d}_2, \end{cases} \quad (7)$$

Our first objective is to design an HGDO that can estimate \mathbf{d}_1 and \mathbf{d}_2 . Our second objective is to use the disturbance estimates and design control laws \mathbf{u}_1 and \mathbf{u}_2 such that the vehicle can follow a desired trajectory $[\mathbf{x}_{1d}^T, \mathbf{x}_{3d}^T]^T$ in the presence of unknown disturbances. Once \mathbf{u}_1 and \mathbf{u}_2 are determined, Ω_i can be calculated using the following expression

$$\begin{bmatrix} \Omega_1^2 \\ \Omega_2^2 \\ \Omega_3^2 \\ \Omega_4^2 \end{bmatrix} = \begin{bmatrix} \frac{1}{4k_T} & 0 & -\frac{1}{2lk_T} & -\frac{1}{4k_Q} \\ \frac{1}{4k_T} & \frac{1}{2lk_T} & 0 & \frac{1}{4k_Q} \\ \frac{1}{4k_T} & 0 & \frac{1}{2lk_T} & -\frac{1}{4k_Q} \\ \frac{1}{4k_T} & -\frac{1}{2lk_T} & 0 & \frac{1}{4k_Q} \end{bmatrix} \begin{bmatrix} u_1 \\ u_2 \\ u_3 \\ u_4 \end{bmatrix}. \quad (8)$$

We assume that the disturbance terms \mathbf{d}_1 and \mathbf{d}_2 and their derivatives are bounded. Let us denote the j -th component of \mathbf{d}_i , $i = \{1, 2\}$ by d_i^j . Then,

$$\|d_i^j\| \leq \delta_i^j, \quad (9)$$

where δ_i^j s denote unknown but finite positive constants and $\|\cdot\|$ is the \mathcal{L}_1 norm defined as $\|\chi(t)\| = \int_0^t |\chi(\alpha)| d\alpha$. The disturbance terms can generally include unknown external

disturbances, gyroscopic effects of rotors, or aerodynamic effects such as drag. The models for gyroscopic effects or drag exist in the literature [40] and one can include them in (4) and (5) to have a more elaborated model. However, these effects can be combined into disturbance terms in each axes, and HGDO can estimate their amplitudes. Therefore, one advantage of using HGDO is reducing the need for complex models.

3 High-Gain Disturbance Observer Design

Our objective in this section is to design an HGDO to estimate \mathbf{d}_1 and \mathbf{d}_2 . Let $\hat{\mathbf{d}}_1$ and $\hat{\mathbf{d}}_2$ be the estimated values of \mathbf{d}_1 and \mathbf{d}_2 . The basic idea behind HGDO is to construct an observer of the following form

$$\begin{cases} \dot{\hat{\mathbf{d}}}_1 = \frac{1}{\varepsilon_1} (\mathbf{d}_1 - \hat{\mathbf{d}}_1), \\ \dot{\hat{\mathbf{d}}}_2 = \frac{1}{\varepsilon_2} (\mathbf{d}_2 - \hat{\mathbf{d}}_2), \end{cases} \quad (10)$$

where $\frac{1}{\varepsilon_1}$ and $\frac{1}{\varepsilon_2}$ are the observer gains. Each equation in (10) constitutes a first-order filter of the form $\frac{1}{\varepsilon_i s + 1}$. By choosing small positive values for ε_i , the settling time of the filter becomes small, and therefore $\hat{\mathbf{d}}_i$ quickly converges to \mathbf{d}_i .

Note that \mathbf{d}_i s are unknown; however, from (7), they can be expressed as follows

$$\begin{cases} \mathbf{d}_1 = \dot{\mathbf{x}}_2 + \mathbf{g} - \mathbf{u}_1, \\ \mathbf{d}_2 = \dot{\mathbf{x}}_4 - \mathbf{f}_2(\mathbf{x}_4) - \mathbf{u}_2. \end{cases} \quad (11)$$

Therefore, one can suggest the following HGDO structure for quadrotor

$$\begin{cases} \dot{\hat{\mathbf{d}}}_1 = \frac{1}{\varepsilon_1} (\dot{\mathbf{x}}_2 + \mathbf{g} - \mathbf{u}_1 - \hat{\mathbf{d}}_1), \\ \dot{\hat{\mathbf{d}}}_2 = \frac{1}{\varepsilon_2} (\dot{\mathbf{x}}_4 - \mathbf{f}_2(\mathbf{x}_4) - \mathbf{u}_2 - \hat{\mathbf{d}}_2). \end{cases} \quad (12)$$

We assume that the initial disturbance estimates are set to zero i.e. $\hat{\mathbf{d}}_i(0) = 0$. The drawback of (12) is the inclusion of derivatives of system states which amplifies the effect of measurement noise. Inspired by [29], we propose an HGDO using auxiliary variables

$$\gamma_1 = \hat{\mathbf{d}}_1 - \frac{\mathbf{x}_2}{\varepsilon_1}, \text{ and } \gamma_2 = \hat{\mathbf{d}}_2 - \frac{\mathbf{x}_4}{\varepsilon_2}, \quad (13)$$

with dynamics given as follows

$$\begin{cases} \dot{\gamma}_1 = -\frac{1}{\varepsilon_1} \left(\gamma_1 + \frac{\mathbf{x}_2}{\varepsilon_1} \right) + \frac{1}{\varepsilon_1} (\mathbf{g}^T - \mathbf{u}_1), \\ \dot{\gamma}_2 = -\frac{1}{\varepsilon_2} \left(\gamma_2 + \frac{\mathbf{x}_4}{\varepsilon_2} \right) + \frac{1}{\varepsilon_2} (-\mathbf{f}_2(\mathbf{x}_4) - \mathbf{u}_2). \end{cases} \quad (14)$$

To establish the convergence results for the observer, let us define the disturbance estimation error as $\tilde{\mathbf{d}}_i = \mathbf{d}_i - \hat{\mathbf{d}}_i$. Taking the derivative of $\tilde{\mathbf{d}}_i$ and using (13) result in

$$\dot{\tilde{\mathbf{d}}}_1 = \dot{\mathbf{d}}_1 - \left(\dot{\gamma}_1 + \frac{\dot{\mathbf{x}}_2}{\varepsilon_1} \right), \quad \dot{\tilde{\mathbf{d}}}_2 = \dot{\mathbf{d}}_2 - \left(\dot{\gamma}_2 + \frac{\dot{\mathbf{x}}_4}{\varepsilon_2} \right). \quad (15)$$

Substituting (14) in (15) leads to

$$\dot{\mathbf{d}}_i = -\frac{1}{\varepsilon_i} \tilde{\mathbf{d}}_i + \dot{\mathbf{d}}_i. \quad (16)$$

The above differential equations can be solved by multiplying both sides with $e^{\frac{1}{\varepsilon_i}t}$ and integrating over $[0, t]$ which yield

$$\tilde{\mathbf{d}}_i(t) = \tilde{\mathbf{d}}_i(0) e^{-\frac{1}{\varepsilon_i}t} + \int_0^t e^{-\frac{1}{\varepsilon_i}(t-\alpha)} \dot{\mathbf{d}}_i(\alpha) d\alpha. \quad (17)$$

Writing (17) in a component-wise form and applying the absolute value operator $|\cdot|$ to both sides lead to

$$\left| \tilde{d}_i^j(t) \right| \leq \left| \tilde{d}_i^j(0) e^{-\frac{1}{\varepsilon_i}t} \right| + \left| \int_0^t e^{-\frac{1}{\varepsilon_i}(t-\alpha)} \dot{d}_i^j(\alpha) d\alpha \right|. \quad (18)$$

According to Holder's inequality [29], $\left| \int_0^t \chi(\tau) d\tau \right| \leq \int_0^t |\chi(\tau)| d\tau$. Therefore,

$$\left| \tilde{d}_i^j(t) \right| \leq \left| \tilde{d}_i^j(0) e^{-\frac{1}{\varepsilon_i}t} \right| + \int_0^t \left| e^{-\frac{1}{\varepsilon_i}(t-\alpha)} \dot{d}_i^j(\alpha) \right| d\alpha. \quad (19)$$

By integrating (19) over $[0, t]$, we get

$$\begin{aligned} \int_0^t \left| \tilde{d}_i^j(\alpha) \right| d\alpha &\leq \int_0^t \left| \tilde{d}_i^j(0) e^{-\frac{1}{\varepsilon_i}\alpha} \right| d\alpha \\ &\quad + \int_0^t \left(\int_0^\beta e^{-\frac{1}{\varepsilon_i}(\beta-\alpha)} \dot{d}_i^j(\alpha) d\alpha \right) d\beta. \end{aligned} \quad (20)$$

The first term on the right-hand side of (20) is bounded by $\varepsilon_i \left| \tilde{d}_i^j(0) \right|$. The second term is equal to $\left\| h(t) * \dot{d}_i^j(t) \right\|$ where $h(t) = e^{-\frac{1}{\varepsilon_i}t}$ and $*$ is the convolution operator. According to Young's convolution theorem [41], $\left\| h(t) * \dot{d}_i^j(t) \right\| \leq \|h(t)\| \left\| \dot{d}_i^j(t) \right\|$. Also, from the definition of \mathcal{L}_1 norm, we have $\|h_i(t)\| = \varepsilon_i$. Therefore,

$$\int_0^t \left| \tilde{d}_i^j(\alpha) \right| d\alpha \leq \varepsilon_i \left| \tilde{d}_i^j(0) \right| + \varepsilon_i \left\| \dot{d}_i^j \right\|. \quad (21)$$

Considering that the left-hand side of (21) is the definition of \mathcal{L}_1 norm for \tilde{d}_i^j and also using (9) result in

$$\left\| \tilde{d}_i^j(t) \right\| \leq \varepsilon_i \left| \tilde{d}_i^j(0) \right| + \delta_i^j, \quad (22)$$

which implies

$$\left\| \tilde{\mathbf{d}}_i(t) \right\| \leq \varepsilon_i \left(\left\| \tilde{\mathbf{d}}_i(0) \right\| + \boldsymbol{\delta}_i \right). \quad (23)$$

As ε_i is a small constant, (22) suggests that the disturbance estimation error is small and bounded for all time and this provides a theoretical verification for the convergence of the proposed HGDO.

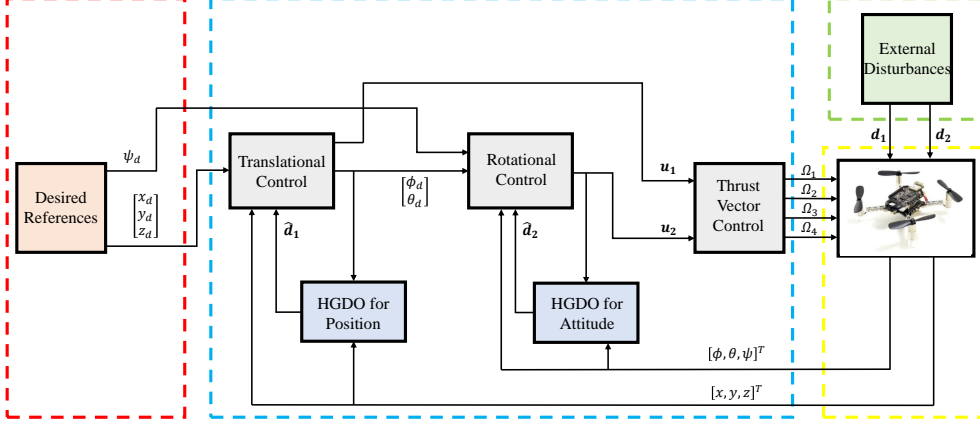


Figure 2: Overview of the control system architecture

4 Controller Design

Our objective in this section is to study how the proposed HGDO can be integrated into the Lyapunov-based control design. We will study SMC design here as an example and establish stability results for the HGDO and the control law. Note that we employ a cascaded structure to handle the underactuation of the quadrotor. As shown in Fig. 2, the outer loop controls the translational dynamics, while the inner loop tackles the rotational dynamics of the vehicle.

Let us start with the definition of tracking errors. Given the desired trajectories $[\mathbf{x}_{1d}^T, \mathbf{x}_{3d}^T]^T$, we define the position tracking error as $\mathbf{e}_1 = \mathbf{x}_{1d} - \mathbf{x}_1$ and the attitude tracking error as $\mathbf{e}_2 = \mathbf{x}_{3d} - \mathbf{x}_3$. Define sliding surfaces as follows

$$\mathbf{s}_i = \dot{\mathbf{e}}_i + \lambda_i \mathbf{e}_i, \quad (24)$$

where $\lambda_i \in \mathbb{R}^3$, $i = \{1, 2\}$ are design parameters with positive components. Let us now consider the following Lyapunov function candidate

$$V = \frac{1}{2} \left(\mathbf{s}_1^T \mathbf{s}_1 + \mathbf{s}_2^T \mathbf{s}_2 + \tilde{\mathbf{d}}_1^T \tilde{\mathbf{d}}_1 + \tilde{\mathbf{d}}_2^T \tilde{\mathbf{d}}_2 \right). \quad (25)$$

Taking the derivative from both sides of (25) and substituting (16) and (24) result in

$$\dot{V} = \mathbf{s}_1^T \dot{\mathbf{s}}_1 + \mathbf{s}_2^T \dot{\mathbf{s}}_2 + \tilde{\mathbf{d}}_1^T \dot{\tilde{\mathbf{d}}}_1 + \tilde{\mathbf{d}}_2^T \dot{\tilde{\mathbf{d}}}_2. \quad (26)$$

Using the tracking error definition and substituting system dynamics (7) yield

$$\begin{aligned} \dot{V} = & \mathbf{s}_1^T (\ddot{\mathbf{x}}_{1d} + \mathbf{g} - \mathbf{u}_1 - \mathbf{d}_1 + \lambda_1 \dot{\mathbf{e}}_1) \\ & + \mathbf{s}_2^T (\ddot{\mathbf{x}}_{3d} - \mathbf{f}_2(\mathbf{x}_4) - \mathbf{u}_2 - \mathbf{d}_2 + \lambda_2 \dot{\mathbf{e}}_2) \\ & + \tilde{\mathbf{d}}_1^T \dot{\tilde{\mathbf{d}}}_1 + \tilde{\mathbf{d}}_2^T \dot{\tilde{\mathbf{d}}}_2. \end{aligned} \quad (27)$$

Let us define the control laws as follows

$$\begin{cases} \mathbf{u}_1 = \ddot{\mathbf{x}}_{1d} + \mathbf{g} - \hat{\mathbf{d}}_1 + \lambda_1 \dot{\mathbf{e}}_1 + \mathbf{k}_1 \text{sgn}(\mathbf{s}_1) + \mathbf{L}_1 \mathbf{s}_1, \\ \mathbf{u}_2 = \ddot{\mathbf{x}}_{3d} - \mathbf{f}_2(\mathbf{x}_4) - \hat{\mathbf{d}}_2 + \lambda_2 \dot{\mathbf{e}}_2 + \mathbf{k}_2 \text{sgn}(\mathbf{s}_2) + \mathbf{L}_2 \mathbf{s}_2, \end{cases} \quad (28)$$

where $\text{sgn}(\cdot)$ denotes the sign function and $\mathbf{k}_i \in \mathbb{R}^3$ and $\mathbf{L}_i \in \mathbb{R}^{3 \times 3}$ are design parameters.

Using (6), the individual components of $\mathbf{u}_1 = [u_x, u_y, u_z]^T$ can be determined as

$$\begin{cases} u_x = \frac{u_1}{m}(\cos \phi \sin \theta \cos \psi + \sin \phi \sin \psi), \\ u_y = \frac{u_1}{m}(\cos \phi \sin \theta \sin \psi - \sin \phi \cos \psi), \\ u_z = \frac{u_1}{m}(\cos \phi \cos \theta). \end{cases} \quad (29)$$

Next, we determine the desired pitch angle ϕ_d , desired roll angle θ_d , and the input to the position controller, u_1 , using (29)

$$\begin{cases} \theta_d = \arctan\left[\frac{u_x \cos \psi_d + u_y \sin \psi_d}{u_z \sin \psi_d - u_y \cos \psi_d}\right], \\ \phi_d = \arctan\left[\cos \theta_d \frac{u_x \sin \psi_d - u_y \cos \psi_d}{u_z}\right], \\ u_1 = \frac{m u_z}{\cos \phi_d \cos \theta_d}. \end{cases} \quad (30)$$

In order to ensure system stability, \mathbf{L}_i must be positive-definite, and \mathbf{k}_i must satisfy a criterion to be detailed shortly. Substituting (28) in (26) leads to

$$\begin{aligned} \dot{V} \leq & -\mathbf{s}_1^T \tilde{\mathbf{d}}_1 - \mathbf{s}_1^T \mathbf{k}_1 \text{sgn}(\mathbf{s}_1) - \mathbf{s}_1^T \mathbf{L}_1 \mathbf{s}_1 \\ & -\mathbf{s}_2^T \tilde{\mathbf{d}}_2 - \mathbf{s}_2^T \mathbf{k}_2 \text{sgn}(\mathbf{s}_2) - \mathbf{s}_2^T \mathbf{L}_2 \mathbf{s}_2 \\ & + \tilde{\mathbf{d}}_1^T \dot{\tilde{\mathbf{d}}}_1 + \tilde{\mathbf{d}}_2^T \dot{\tilde{\mathbf{d}}}_2. \end{aligned} \quad (31)$$

For the last two terms in (31), we use (16) to write

$$\tilde{\mathbf{d}}_1^T \dot{\tilde{\mathbf{d}}}_1 + \tilde{\mathbf{d}}_2^T \dot{\tilde{\mathbf{d}}}_2 = -\frac{1}{\varepsilon_1} \tilde{\mathbf{d}}_1^T \tilde{\mathbf{d}}_1 + \tilde{\mathbf{d}}_1^T \dot{\tilde{\mathbf{d}}}_1 - \frac{1}{\varepsilon_2} \tilde{\mathbf{d}}_2^T \tilde{\mathbf{d}}_2 + \tilde{\mathbf{d}}_2^T \dot{\tilde{\mathbf{d}}}_2. \quad (32)$$

For $\tilde{\mathbf{d}}_i^T \dot{\tilde{\mathbf{d}}}_i$ terms, we can use (9) and (23) to find upper bounds ρ_i as follows

$$\tilde{\mathbf{d}}_i^T \dot{\tilde{\mathbf{d}}}_i \leq \varepsilon_i \left(\left\| \tilde{\mathbf{d}}_i(0) \right\| + \|\boldsymbol{\delta}_i\| \right) \|\boldsymbol{\delta}_i\| \leq \rho_i \quad (33)$$

By substituting (16), (32), and (33) in (31), we get

$$\begin{aligned} \dot{V} \leq & \varepsilon_1 \|\mathbf{s}_1\| \left(\left\| \tilde{\mathbf{d}}_1(0) \right\| + \|\boldsymbol{\delta}_1\| - \frac{1}{\varepsilon_1} \mathbf{k}_1 \right) - \mathbf{s}_1^T \mathbf{L}_1 \mathbf{s}_1 \\ & + \varepsilon_2 \|\mathbf{s}_2\| \left(\left\| \tilde{\mathbf{d}}_2(0) \right\| + \|\boldsymbol{\delta}_2\| - \frac{1}{\varepsilon_2} \mathbf{k}_2 \right) - \mathbf{s}_2^T \mathbf{L}_2 \mathbf{s}_2 \\ & - \frac{1}{\varepsilon_1} \tilde{\mathbf{d}}_1^T \tilde{\mathbf{d}}_1 - \frac{1}{\varepsilon_2} \tilde{\mathbf{d}}_2^T \tilde{\mathbf{d}}_2 + \rho_1 + \rho_2. \end{aligned} \quad (34)$$

Let us now choose \mathbf{k}_i in a way that its components satisfy

$$k_i^j > \varepsilon_i \left(\left| \tilde{d}_i^j(0) \right| + \delta_i^j \right). \quad (35)$$

Then, we can write

$$\begin{aligned} \dot{V} \leq & -\mathbf{s}_1^T \lambda_{\max}(\mathbf{L}_1) \mathbf{s}_1 - \mathbf{s}_2^T \lambda_{\max}(\mathbf{L}_2) \mathbf{s}_2 \\ & - \frac{1}{\varepsilon_1} \tilde{\mathbf{d}}_1^T \tilde{\mathbf{d}}_1 - \frac{1}{\varepsilon_2} \tilde{\mathbf{d}}_2^T \tilde{\mathbf{d}}_2 + \rho_1 + \rho_2, \end{aligned} \quad (36)$$

where $\lambda_{\max}(\cdot)$ denotes the largest eigenvalue. We can now write

$$\dot{V} \leq -\kappa V + \rho, \quad (37)$$

where $\kappa = \min \left\{ \lambda_{\max}(\mathbf{L}_1), \lambda_{\max}(\mathbf{L}_2), \frac{1}{\varepsilon_1}, \frac{1}{\varepsilon_2} \right\}$ and $\rho = \rho_1 + \rho_2$. Taking steps similar to (15)-(17), we get

$$V(t) \leq e^{-\kappa t} V(0) + \int_0^t e^{-\kappa(t-\alpha)} \rho(\alpha) d\alpha, \quad (38)$$

which implies V is bounded. Subsequently, \mathbf{s}_i s are bounded. This means that the tracking errors are bounded. Therefore, with the control law (28) and (35), the vehicle trajectory will remain in an adjustable neighborhood of the desired trajectory.

One benefit of HGDO becomes clear in (35). Note that ε_i needs to be small to ensure fast disturbance estimation. This means that $\varepsilon_i \left(\left| \tilde{d}_i^j(0) \right| + \delta_i^j \right)$ have relatively small values, and thus, with small gains k_i^j the stability condition (35) can be satisfied. Small gains k_i^j can potentially lead to smaller control efforts.

It is worth noting that the control laws in (28) can lead to chattering due to the discontinuity of the sign function. Therefore, for practical implementations, we will replace the sign function with saturation function $\text{sat} \left(\frac{\mathbf{s}_i}{\mu} \right)$ where the slope of its linear portion is $\frac{1}{\mu}$. When $s_i^j > \mu$, the above stability results hold. Therefore, the system states will remain bounded even when the saturation function is used.

One major concern about HGO- and HGDO-based controllers is the peaking phenomenon that could result from very small ε values. In [27], it is shown that passing the computed control signal from a saturation function can resolve the issue. As such, in our experiments presented in the next section, we will apply a saturation function to the computed signal to address the peaking phenomenon.

5 Experiments

This section presents the results of our simulation and laboratory experiments to evaluate the effectiveness of the proposed HGDO-based control. Our primary focus will be on laboratory experiments. However, simulations are necessary to assess the accuracy of disturbance estimations; as it is otherwise challenging due to the difficulty of measuring the exact values of disturbances in practice.

To highlight the benefits gained by HGDO, we compare our HGDO+SMC approach with the uncertainty and disturbance estimator method (UDE) [19], SMC-only, and also with one of the recent DO-based control methods [10] that have tackled a similar problem.

The vehicle under consideration throughout the experiments was a Crazyflie 2.1, flying in a controlled environment equipped with the lighthouse positioning system [42]. All the flight control computations were conducted on an external computer using MATLAB and transferred to the vehicle in real-time using Robot Operating System (ROS).

The parameter values for the vehicle, SMC, and HGDO used throughout simulations and real experiments are given in Tab. 1. For tuning the SMC parameters, we used the genetic algorithm where the objective function was the integral of squared tracking errors. Once the SMC parameters were optimized, we tuned the HGDO parameters in a quick trial-and-error process. To show the effect of ε in HGDO performance, we present results for three different values of 0.01, 0.04, and 0.08.

Table 1: Parameter values used during experiments

Parameter	Value
<i>a) Vehicle Parameters:</i>	
m	28 g
\mathbf{J}	$\text{diag}(1.4, 1.4, 2.17) \times 10^{-5} \text{ kgm}^2$
k_T	$2.88 \times 10^{-8} \text{ N s}^2$
k_Q	$7.24 \times 10^{-10} \text{ Nm s}^2$
l	92 mm
<i>b) SMC Parameters:</i>	
λ_1	$[0.3580, 0.5058, 0.3405]^T$
λ_2	$[0.3580, 0.5058, 0.3405]^T$
\mathbf{k}_1	$[-5.2608, -5.0176, -5.4351]^T$
\mathbf{k}_2	$[-8.0568, -13.6547, -1.8914]^T$
\mathbf{L}_1	$\text{diag}(-2.6304, -2.5088, -2.7176)$
\mathbf{L}_2	$\text{diag}(-4.0284, -6.8274, -0.9457)$
<i>c) HGDO Parameters:</i>	
ε_1	0.01
ε_2	0.01

5.1 Simulations

The desired trajectories of the quadrotor were chosen as $\mathbf{x}_{1d} = [0.5 \sin(\frac{2\pi t}{40}), \sin(\frac{2\pi t}{40}) \cos(\frac{2\pi t}{40}), 0.5]^T$ and $\mathbf{x}_{3d} = [0, 0, 0]^T$. For external disturbances, we used a sinusoidal disturbance with the maximum frequency of 4 Hz as $d = 0.05[\sin(8\pi t) + \sin(2.5\pi(t-3)) + 1.5 \sin(2\pi(t+7)) + 2 \sin(0.4\pi(t-9)) + \sin(0.2\pi t) + 0.5 \sin(0.08\pi(t+1)) + \sin(0.07\pi(t+1.5)) + 0.5 \sin(0.05\pi(t+2))] + 4$. This disturbance is taken from [10], with the addition of a $\sin(8\pi t)$ term to account for relatively higher frequency disturbances. We also used the Dryden wind turbulence model [43], a widely recognized model for its applicability in capturing real-world disturbances.

Figures 3 and 4 compare the actual disturbance and the estimated values using HGDO and the DOs given in [10] and [19]. In Fig. 3, among HGO results with different gains, the best disturbance estimation results correspond to $\varepsilon = 0.01$, as expected. The differences are clear in both convergence speed and estimation error. It is easy to verify that the value of ε directly influences the speed and accuracy of estimation, providing an easy way to calibrate the DO.

Comparing the HGDO with the method in [10], it is evident that even with $\varepsilon = 0.08$, the HGDO exhibits higher convergence speed. In terms of estimation accuracy, the difference between the method in [10] and HGDO with $\varepsilon = 0.08$ becomes insignificant over time; however, when ε is set to 0.01, HGDO has a clear advantage.

The UDE method described in [19] exhibits a considerable overshoot at the start of the simulation. While this overshoot signifies the method's ability to address disturbances promptly, it could present practical difficulties, particularly in situations requiring precise and immediate adherence to a set trajectory without initial deviations. Once the transient behavior is passed, the UDE's estimation accuracy is comparable to HGDO with $\varepsilon = 0.01$; however, the HGDO has a smaller overshoot at the initial phase.

Concerning Fig. 4, although the disturbance generated by the Dryden model is stochastic; the disturbance estimates have converged to the actual disturbance values only after a short

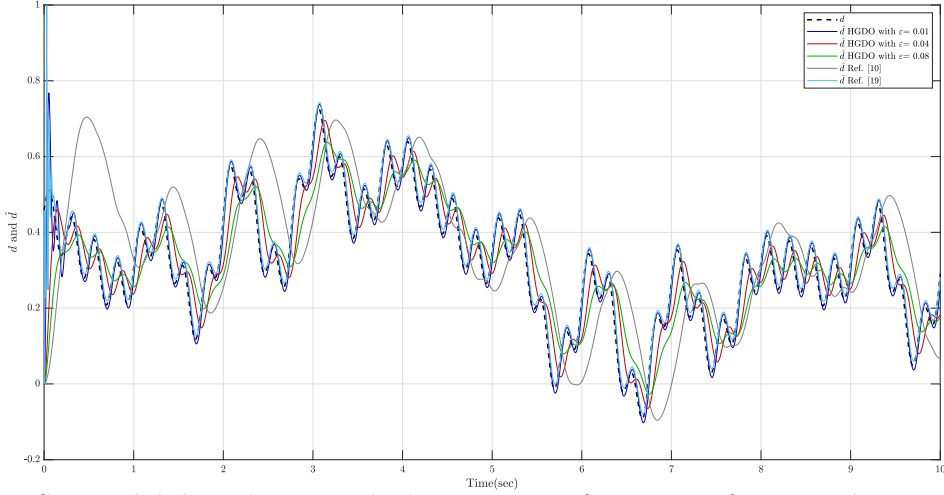


Figure 3: Sinusoidal disturbance with the maximum frequency of 4 Hz and its estimation

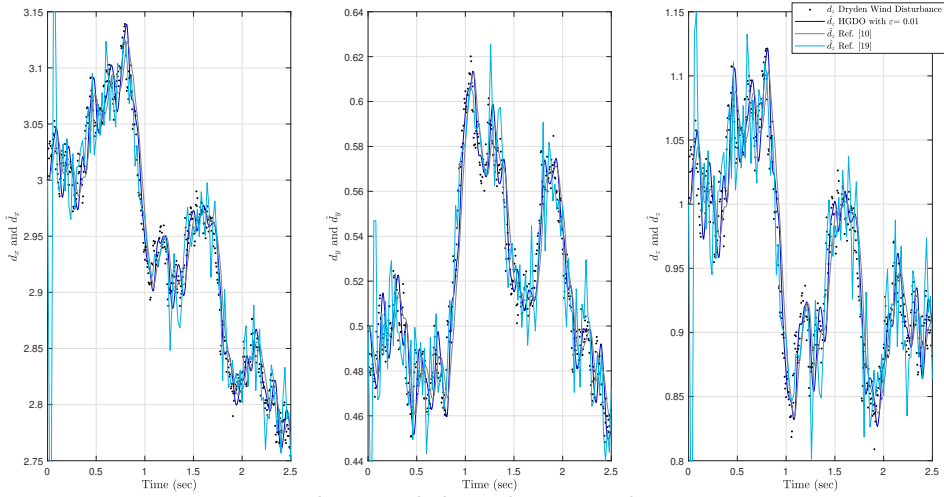


Figure 4: Dryden wind disturbance and its estimation

transient time; however, the HGDO estimates are much closer to the actual disturbances compared to the two alternative methods. Such a fast and accurate disturbance estimation presents a significant advantage in disturbance compensation and robust trajectory tracking.

To investigate the HGDO performance in the presence of noise, we used white Gaussian measurement noise in our simulations, conducting three trials, each with a different noise power (0.001, 0.01, and 0.1 W) as shown in Fig. 5. HGOs are known to be sensitive to measurement noise, and this is evident in simulation results, especially for the highest noise power considered. However, the estimation results are still reasonable, with an accuracy comparable to our benchmark methods with no measurement noise. However, if the jitter in HGDO estimations is deemed to be problematic for a certain application, there exists a large body of literature on dealing with measurement noise for HGOs, e.g., by switching between two gains [44], gain adaptation [45], or integration with Kalman filter [28]. Note that there exists a formal mathematical guarantee for the boundedness of HGO estimation errors in the presence of bounded measurement noise, detailed in Theorem 8.1 of [27].

Figure 6 depicts the 3D plot of the vehicle trajectory versus the desired trajectory in the time interval $[0, 40s]$. Note that, in each trial, the vehicle completes the lemniscate

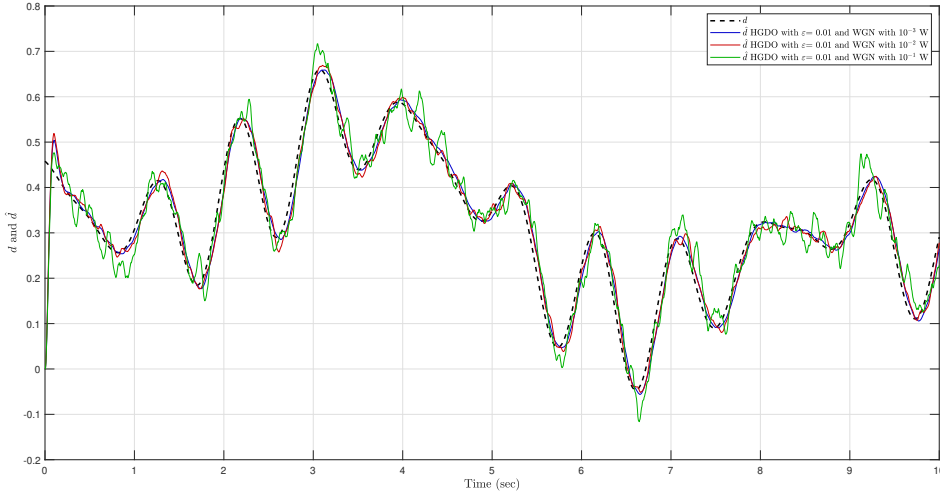


Figure 5: Sinusoidal disturbance and its estimation in the presence of noise.

figure twice. The largest tracking error is associated with the SMC-only controller. When DO is introduced, the trajectory tracking is much improved; however, the convergence to the desired trajectory is noticeably slower with the DOs in [10] and [19]. This likely stems from the slower convergence of disturbance estimations with these methods compared to the HGDO, as confirmed in Figs. 3 and 4.

Figure 7 presents a closer look at the vehicle position. The magnified windows provide a means to compare the magnitude of tracking errors. Notably, HGDO with $\varepsilon = 0.01$ exhibits a remarkably near-zero tracking error. While tracking errors degrade by the increase in ε , the worst HGDO-based results still have faster convergence and similar tracking errors compared to the three alternative methods.

5.2 Laboratory Experiments

Scenario 1: Tracking a lemniscate trajectory

In this scenario, the vehicle tracks a lemniscate path similar to the one mentioned in simulations. An external fan generates a wind disturbance with a speed of 4 km/h in the vicinity of the path, and the vehicle undergoes a non-uniform disturbance as it completes the path. Figure 8 presents the vehicle trajectory for the different methods. Note that the vehicle completes the path twice to have a rough assessment of the repeatability of the results. A closer look at the position states and the tracking error in Figs. 9 and 10 highlight the superiority of HGDO+SMC, both in terms of convergence speed and tracking error.

We also study the vehicle's attitude in this scenario, targeting a desired trajectory of $[\psi, \phi, \theta]^T = [0, 0, 0]^T$. Comparing HGDO+SMC results with SMC-only and [10] in Fig. 11, it is clear that HGDO+SMC outperforms the alternative methods.

To provide a quantitative assessment of the performance of the controllers, we tabulate the root mean square (RMS) of position and attitude tracking errors of the different control strategies in Tab. 2. First, the SMC-only results have the highest error values, highlighting the benefits of adding a DO to achieve higher tracking accuracy. Second, comparing DO-based results shows that all HGDO+SMC results, even with $\varepsilon = 0.08$, exhibit smaller errors compared to [10]. As expected, the HGDO with $\varepsilon = 0.01$ has a clear advantage over all the

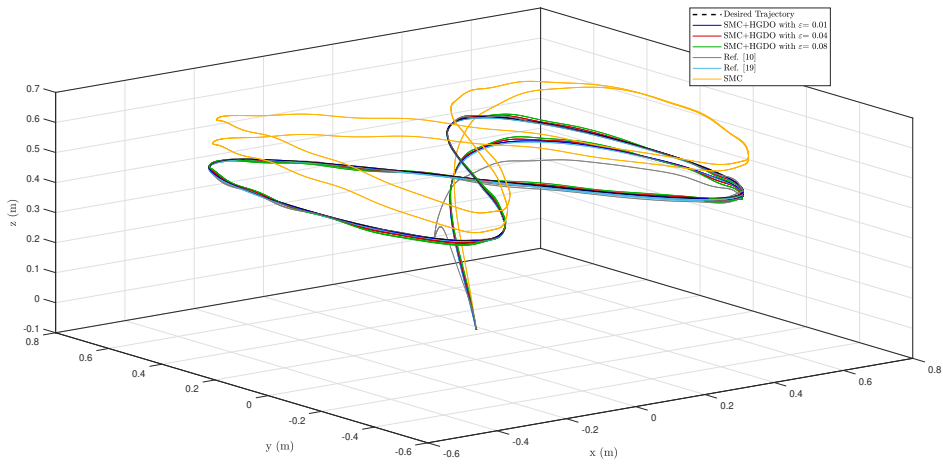


Figure 6: 3D plot of the vehicle trajectory compared to the desired trajectory in the simulation study.

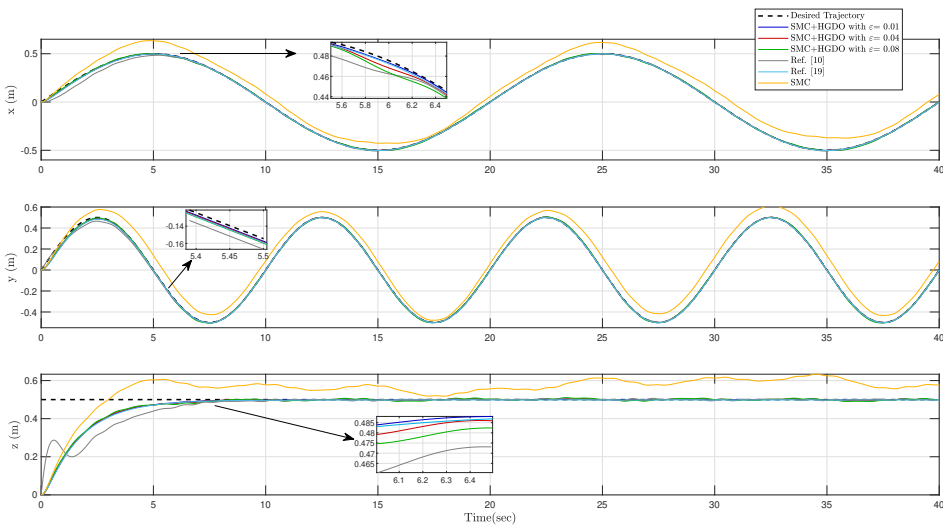


Figure 7: Desired and actual vehicle position trajectories in the simulation study.

other alternatives.

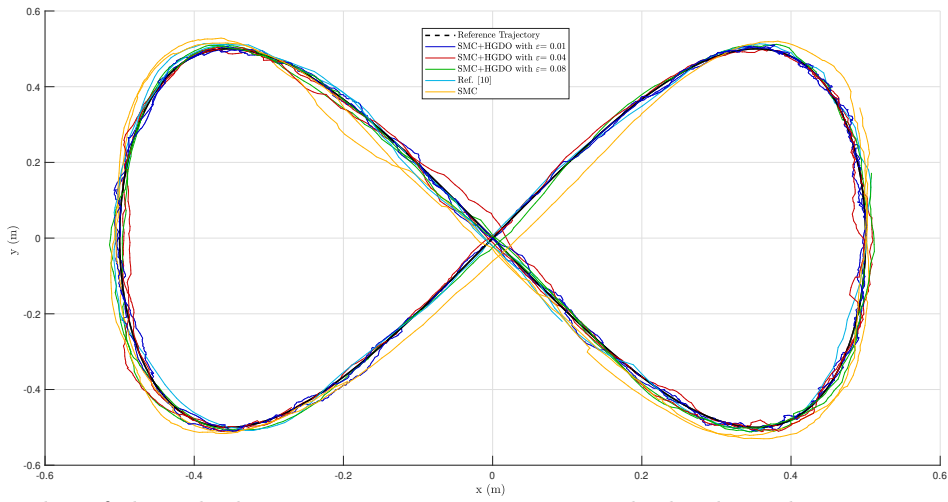


Figure 8: 2D plot of the vehicle trajectory in comparison with the desired trajectory in tracking a lemniscate trajectory.

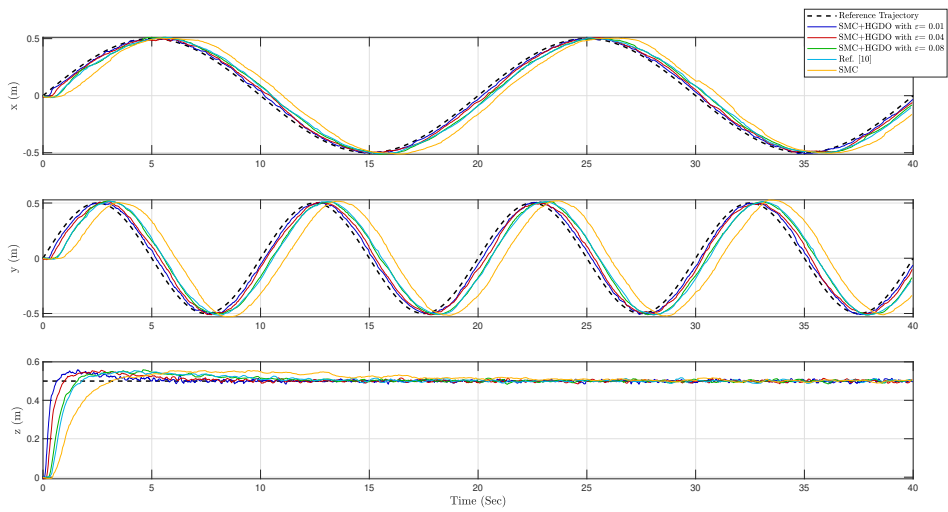


Figure 9: Desired and actual vehicle position trajectories in tracking a lemniscate trajectory scenario.

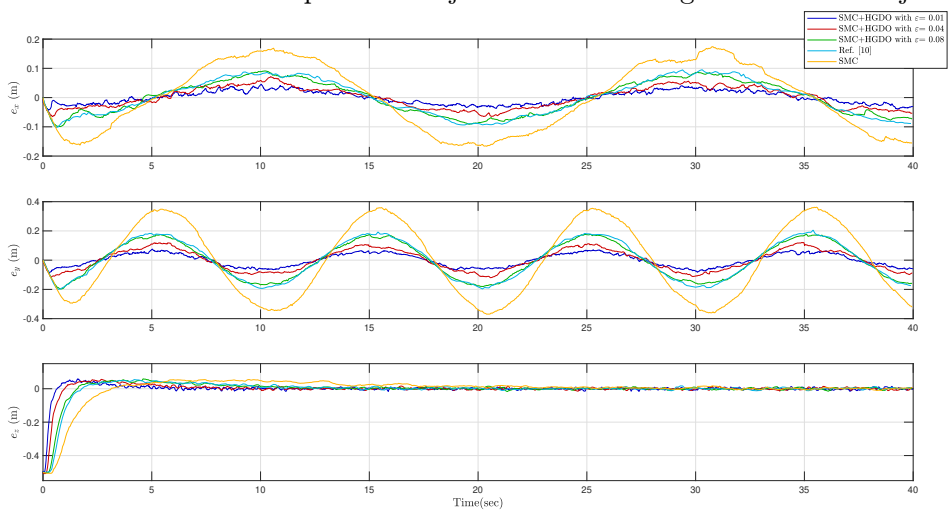


Figure 10: Position tracking error in tracking a lemniscate trajectory scenario.

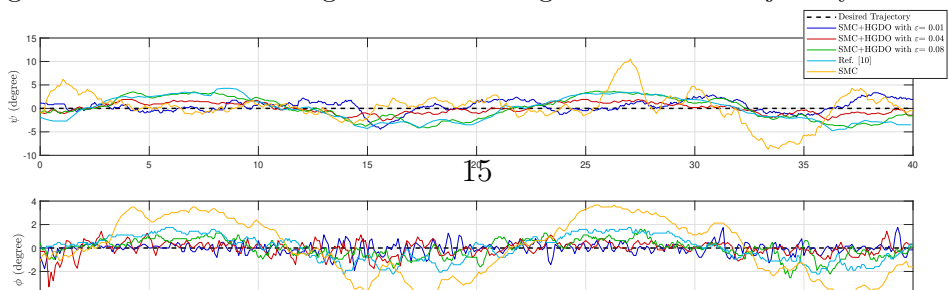


Table 2: Root mean square of position and attitude tracking errors in tracking a lemniscate trajectory.

Parameter	SMC+HGDO with $\varepsilon= 0.01$	SMC+HGDO with $\varepsilon= 0.04$	SMC+HGDO with $\varepsilon= 0.08$	Ref. [10]	SMC
x	0.022	0.035	0.056	0.060	0.111
y	0.044	0.070	0.119	0.128	0.242
z	0.037	0.050	0.064	0.072	0.018
ψ	0.021	0.032	0.041	0.044	0.054
ϕ	0.008	0.010	0.013	0.019	0.041
θ	0.006	0.008	0.009	0.012	0.018

Scenario 2: Ground effect

In this scenario, we conducted a comprehensive evaluation of the vehicle’s performance in close proximity to the ground, maintaining a minimal altitude of just 10 cm while executing a lemniscate trajectory, with the objective of ensuring that the vehicle’s attitude remains stable and near zero throughout the flight. We did not use an external fan in this case to focus on another form of external disturbance that exists due to the airflow distortion near the ground known as the ground effect.

Figures 12 - 14 illustrate the results of trajectory tracking for position, while Fig. 16 depicts the results for attitude tracking. Once again, these figures confirm the superior performance achieved through the use of HGDO+SMC. Fig. 15 presents the real-time estimation of disturbances encountered during flight including the ground effect. Interestingly, the disturbance estimate along the z -axis is relatively larger, which can be explained by the presence of the ground effect.

Table 3 compares the RMS values of position and attitude tracking errors for different control strategies in this scenario, again, showing the superiority of HGDO+SMC to other methods.

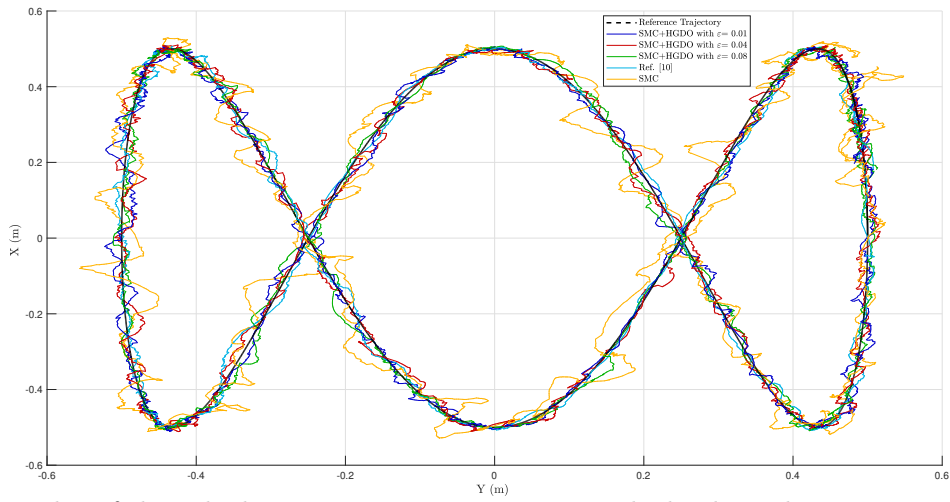


Figure 12: 2D plot of the vehicle trajectory in comparison with the desired trajectory in the ground effect scenario.

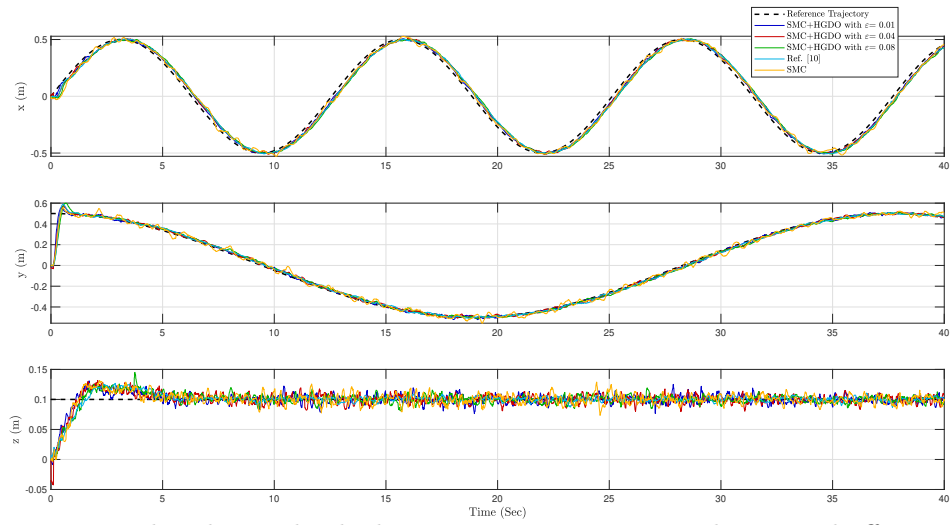


Figure 13: Desired and actual vehicle position trajectories in the ground effect scenario.

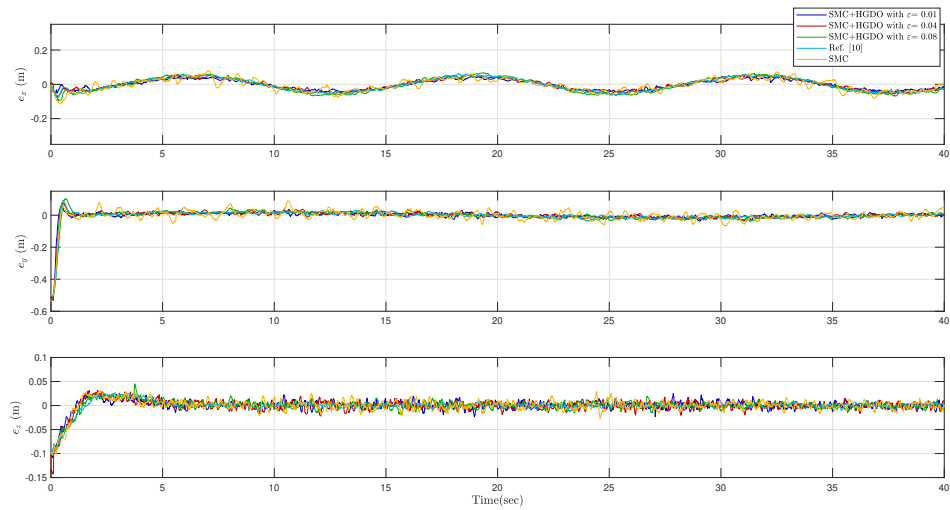


Figure 14: Position tracking error in the ground effect scenario.

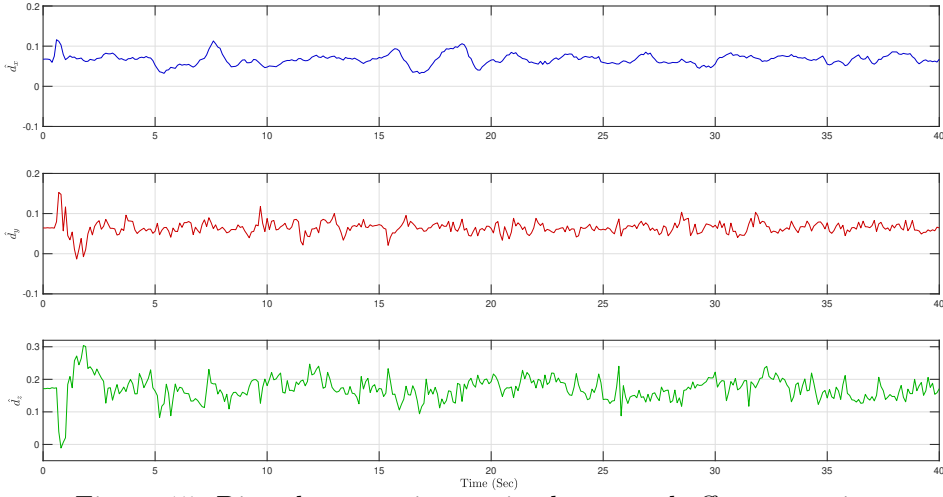


Figure 15: Disturbance estimates in the ground effect scenario.

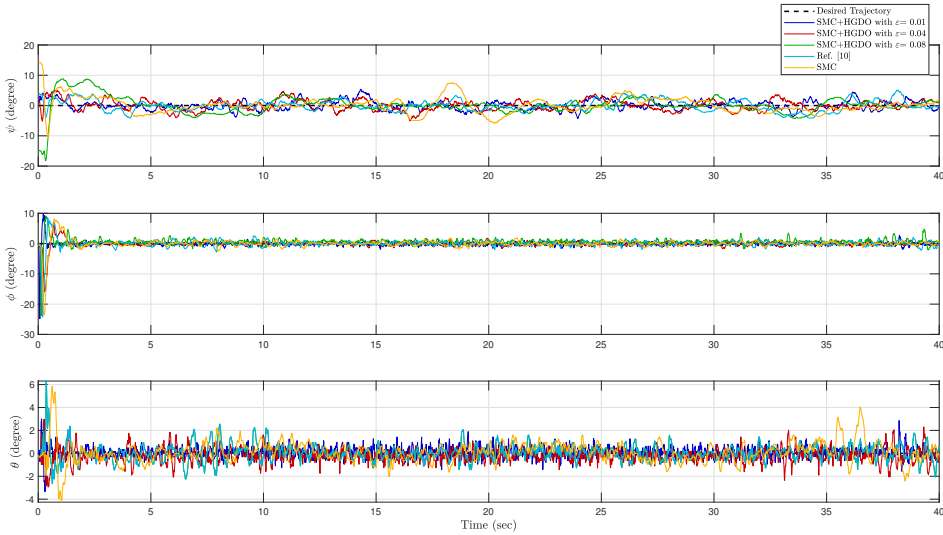


Figure 16: Desired and actual vehicle attitude in the ground effect scenario.

Table 3: Root mean square of position and attitude tracking errors in the ground effect scenario.

Parameter	SMC+HGDO with $\varepsilon = 0.01$	SMC+HGDO with $\varepsilon = 0.04$	SMC+HGDO with $\varepsilon = 0.08$	Ref. [10]	SMC
x	0.028	0.033	0.036	0.037	0.042
y	0.037	0.041	0.043	0.042	0.044
z	0.012	0.013	0.014	0.013	0.014
ψ	0.026	0.030	0.031	0.031	0.044
ϕ	0.016	0.020	0.023	0.024	0.028
θ	0.007	0.010	0.012	0.013	0.016

Scenario 3: Hovering control

In this scenario, the vehicle takes off from the origin, flies to point $[0.5, 0.5, 0.5]^T$, and hovers at this point, all with the aim of preserving the vehicle's attitude in a stable and nearly zero state throughout the entire flight duration. There is an external fan in the vicinity of the hover point generating a wind disturbance with a speed of 4 km/h . In the hover point, the vehicle resists the disturbance and holds its position. Figure 17 shows the position tracking error for each experimental trial. It is clear that, with all methods, the vehicle has

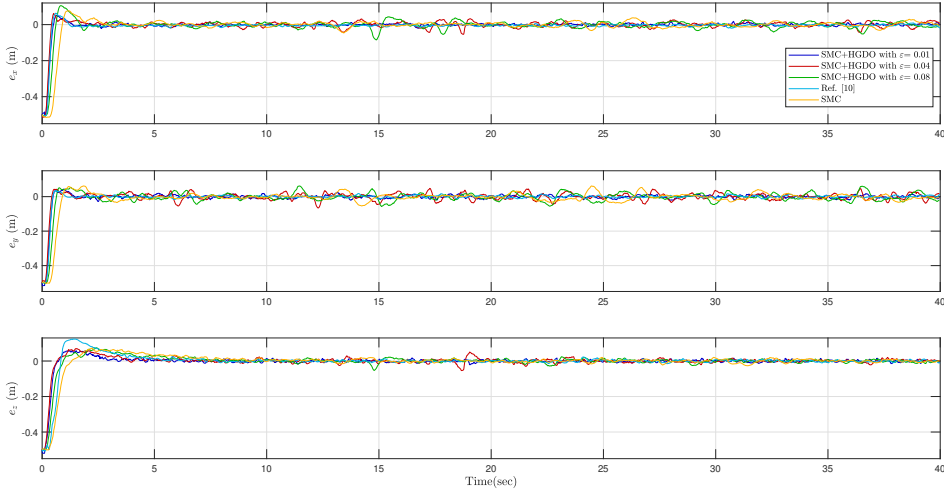


Figure 17: Position tracking error in the hovering scenario.

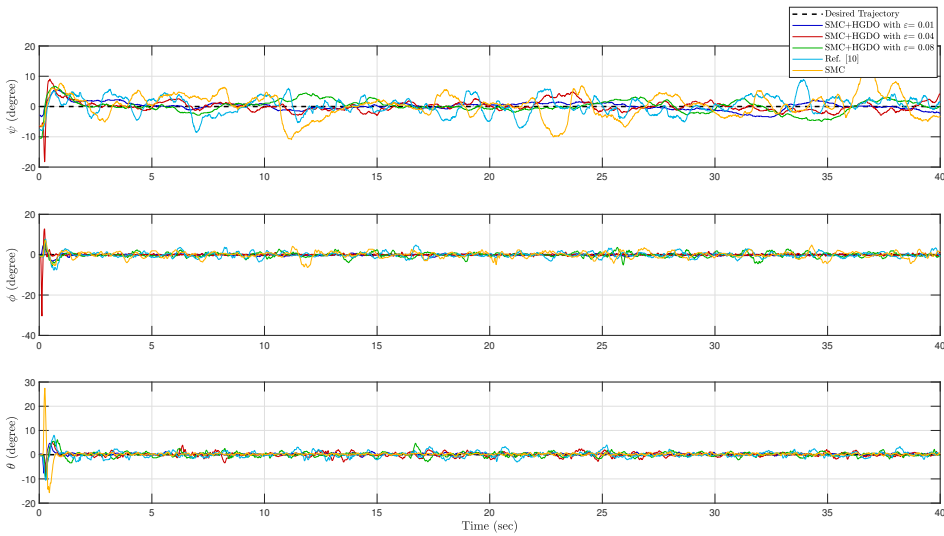


Figure 18: Desired and actual vehicle attitude in the hovering scenario.

successfully reached to hover point and held its position despite the disturbances. However, when compared to the other two methods, HGDO+SMC exhibits reduced fluctuations in the hover point.

In this experiment, all the desired rotational states were set to zero. However, the external fan was generating disturbances in the rotational states. Fig. 18 showcases the attitude trajectory in each trial, confirming a better disturbance rejection for the rotational states using HGDO, especially with $\varepsilon = 0.01$. Table 4 compares the RMS of position and attitude tracking errors for different control strategies in this scenario.

6 Conclusion

This study developed an HGDO for robust trajectory tracking of quadrotors. Our theoretical results established that (i) HGDO can guarantee the boundedness of disturbance estimation error with a short transient time, and (ii) HGDO combined with Lyapunov-based controllers can guarantee the boundedness of position and attitude tracking errors. Our experimental results conformed with theoretical results and demonstrated that adding HGDO to a flight

Table 4: Root mean square of position and attitude tracking errors in the hovering scenario.

Parameter	SMC+HGDO with $\varepsilon=0.01$	SMC+HGDO with $\varepsilon=0.04$	SMC+HGDO with $\varepsilon=0.08$	Ref. [10]	SMC
x	0.042	0.044	0.055	0.044	0.065
y	0.043	0.044	0.055	0.043	0.064
z	0.045	0.045	0.054	0.060	0.065
ψ	0.023	0.033	0.036	0.054	0.069
ϕ	0.008	0.018	0.021	0.024	0.027
θ	0.010	0.016	0.019	0.022	0.026

controller significantly improves the quadrotor’s robustness against external disturbances.

Note that despite HGDO’s several desirable properties, its use in quadrotor control has remained minimal in the past. Besides the fact that the advantages of HGDO were not thoroughly studied for quadrotors before this paper, there could be skepticism attributed to the sensitivity of conventional HGDOs to measurement noise. However, our HGDO-based flight control was capable of handling the typical measurement noise present in inertial measurement units and motion capture systems in a common research vehicle. Therefore, we argue that HGDO is a simple, easy-to-tune, and computationally efficient module that can be added to conventional quadrotor flight control approaches to boost system robustness. The HGDO-based control performance can be further improved by explicitly considering measurement noise, high-frequency disturbances, and the limitations of sensors and actuators in the design. Future work in HGDO can delve into these topics to further strengthen HGDO advantages for quadrotor control.

References

- [1] David Galway, Jason Etele, and Giovanni Fusina. Modeling of the urban gust environment with application to autonomous flight. In *AIAA Atmospheric Flight Mechanics Conference and Exhibit*, page 6565, 2008. doi: 10.2514/6.2008-6565.
- [2] Xiang He and Kam K Leang. Quasi-steady in-ground-effect model for single and multi-rotor aerial vehicles. *AIAA Journal*, 58(12):5318–5331, 2020. doi: 10.2514/1.J059223.
- [3] Joshua C Nathanael, Chung-Hung John Wang, and Kin Huat Low. Numerical studies on modeling the near-and far-field wake vortex of a quadrotor in forward flight. *Proceedings of the Institution of Mechanical Engineers, Part G: Journal of Aerospace Engineering*, 236(6):1166–1183, 2022. doi: 10.1177/09544100211029074.
- [4] Melissa Greeff and Angela P Schoellig. Flatness-based model predictive control for quadrotor trajectory tracking. In *2018 IEEE/RSJ International Conference on Intelligent Robots and Systems (IROS)*, pages 6740–6745. IEEE, 2018. doi: 10.1109/IROS.2018.8594012.
- [5] Qiyuan Zhang, Xiaona Song, Shuai Song, and Vladimir Stojanovic. Finite-time sliding mode control for singularly perturbed pde systems. *Journal of the Franklin Institute*, 360(2):841–861, 2023. doi: 10.1016/j.jfranklin.2022.11.037.

- [6] Fang Nan, Sihao Sun, Philipp Foehn, and Davide Scaramuzza. Nonlinear mpc for quadrotor fault-tolerant control. *IEEE Robotics and Automation Letters*, 7(2):5047–5054, 2022. doi: 10.1109/LRA.2022.3154033.
- [7] Rong Xu and Umit Ozguner. Sliding mode control of a quadrotor helicopter. In *Proceedings of the 45th IEEE Conference on Decision and Control*, pages 4957–4962. IEEE, 2006. doi: 10.1109/CDC.2006.377588.
- [8] Zhiwei Hou, Peng Lu, and Zhangjie Tu. Nonsingular terminal sliding mode control for a quadrotor uav with a total rotor failure. *Aerospace Science and Technology*, 98:105716, 2020. doi: 10.1016/j.ast.2020.105716.
- [9] En-Hui Zheng, Jing-Jing Xiong, and Ji-Liang Luo. Second order sliding mode control for a quadrotor uav. *ISA transactions*, 53(4):1350–1356, 2014. doi: 10.1016/j.isatra.2014.03.010.
- [10] Meisam Kabiri, Hajar Atrianfar, and Mohammad Bagher Menhaj. 3d trajectory tracking control for a thrust-propelled vehicle with time-varying disturbances. *International Journal of Control, Automation and Systems*, 17:1978–1986, 2019. doi: 10.1007/s12555-018-0331-3.
- [11] Paul De Monte and Boris Lohmann. Position trajectory tracking of a quadrotor helicopter based on l1 adaptive control. In *2013 European Control Conference (ECC)*, pages 3346–3353. IEEE, 2013. doi: 10.1515/auto-2013-1035.
- [12] Xiaona Song, Chenglin Wu, Vladimir Stojanovic, and Shuai Song. 1 bit encoding–decoding-based event-triggered fixed-time adaptive control for unmanned surface vehicle with guaranteed tracking performance. *Control Engineering Practice*, 135:105513, 2023. doi: 10.1016/j.conengprac.2023.105513.
- [13] Priya L Donti, Melrose Roderick, Mahyar Fazlyab, and J Zico Kolter. Enforcing robust control guarantees within neural network policies. *arXiv preprint arXiv:2011.08105*, 2020. doi: 10.48550/arXiv.2011.08105.
- [14] Haoran Han, Jian Cheng, Zhilong Xi, and Bingcai Yao. Cascade flight control of quadrotors based on deep reinforcement learning. *IEEE Robotics and Automation Letters*, 7(4):11134–11141, 2022. doi: 10.1109/LRA.2022.3196455.
- [15] Kamal Youcef-Toumi and Osamu Ito. A time delay controller for systems with unknown dynamics. In *1988 American Control Conference*, pages 904–913, 1988. doi: 10.23919/ACC.1988.4789852.
- [16] Jeong Geun Lim and Seul Jung. Altitude control of a quad-rotor system by using a time-delayed control method. *Journal of Institute of Control, Robotics and Systems*, 20(7):724–729, 2014. doi: 10.5302/J.ICROS.2014.13.1947.
- [17] Charles E Hall and Yuri B Shtessel. Sliding mode disturbance observer-based control for a reusable launch vehicle. *Journal of guidance, control, and dynamics*, 29(6):1315–1328, 2006. doi: 10.2514/1.20151.

- [18] Di Shi, Zhong Wu, and Wusheng Chou. Generalized extended state observer based high precision attitude control of quadrotor vehicles subject to wind disturbance. *IEEE Access*, 6:32349–32359, 2018. doi: 10.1109/ACCESS.2018.2842198.
- [19] SE Talole and SB Phadke. Model following sliding mode control based on uncertainty and disturbance estimator. *ASME Journal of Dynamic Systems, Measurement, and Control*, 130(3):034501, 2008.
- [20] TS Chandar and SE Talole. Improving the performance of ude-based controller using a new filter design. *Nonlinear Dynamics*, 77(3):753–768, 2014. doi: 10.1007/s11071-014-1337-x.
- [21] Qing-Chang Zhong and David Rees. Control of uncertain lti systems based on an uncertainty and disturbance estimator. *J. Dyn. Sys., Meas., Control*, 126(4):905–910, 2004. doi: 10.1115/1.1850529.
- [22] Chenhui Zhou, Hongfeng Tao, Yiyang Chen, Vladimir Stojanovic, and Wojciech Paszke. Robust point-to-point iterative learning control for constrained systems: A minimum energy approach. *International Journal of Robust and Nonlinear Control*, 32(18):10139–10161, 2022. doi: 10.1002/rnc.6354.
- [23] Weisheng Liang, Zheng Chen, and Bin Yao. Geometric adaptive robust hierarchical control for quadrotors with aerodynamic damping and complete inertia compensation. *IEEE Transactions on Industrial Electronics*, 69(12):13213–13224, 2021. doi: 10.1109/TIE.2021.3137615.
- [24] Nuradeen Fethalla, Maarouf Saad, Hannah Michalska, and Jawhar Ghommam. Robust observer-based dynamic sliding mode controller for a quadrotor uav. *IEEE access*, 6: 45846–45859, 2018. doi: 10.1109/ACCESS.2018.2866208.
- [25] Deqing Huang, Tianpeng Huang, Na Qin, Yanan Li, and Yong Yang. Finite-time control for a uav system based on finite-time disturbance observer. *Aerospace Science and Technology*, 129:107825, 2022. doi: 10.1016/j.ast.2022.107825.
- [26] Vladimir Stojanović. Fault-tolerant control of a hydraulic servo actuator via adaptive dynamic programming. *Mathematical Modelling and Control*, 2023. doi: 10.3934/mmc.2023016.
- [27] Hassan K Khalil. *High-gain observers in nonlinear feedback control*. SIAM, 2017. doi: 10.1002/rnc.3051.
- [28] Nicolas Boizot, Eric Busvelle, and Jean-Paul Gauthier. An adaptive high-gain observer for nonlinear systems. *Automatica*, 46(9):1483–1488, 2010. doi: 10.1016/j.automatica.2010.06.004.
- [29] Daehee Won, Wonhee Kim, Donghoon Shin, and Chung Choo Chung. High-gain disturbance observer-based backstepping control with output tracking error constraint for electro-hydraulic systems. *IEEE Transactions on Control Systems Technology*, 23(2): 787–795, 2015. doi: 10.1109/TCST.2014.2325895.

- [30] Hassan K Khalil. Extended high-gain observers as disturbance estimators. *SICE Journal of Control, Measurement, and System Integration*, 10(3):125–134, 2017. doi: 10.9746/jcmsi.10.125.
- [31] Connor J Boss, Joonho Lee, and Jongeun Choi. Uncertainty and disturbance estimation for quadrotor control using extended high-gain observers: Experimental implementation. In *Dynamic Systems and Control Conference*, volume 58288, page V002T01A003. American Society of Mechanical Engineers, 2017. doi: 10.1115/DSCC2017-5204.
- [32] Kai Zhao, Jinhui Zhang, Dailiang Ma, and Yuanqing Xia. Composite disturbance rejection attitude control for quadrotor with unknown disturbance. *IEEE Transactions on Industrial Electronics*, 67(8):6894–6903, 2019. doi: 10.1109/TIE.2019.2937065.
- [33] Qi Lu, Beibei Ren, and Siva Parameswaran. Uncertainty and disturbance estimator-based global trajectory tracking control for a quadrotor. *IEEE/ASME Transactions on Mechatronics*, 25(3):1519–1530, 2020. doi: 10.1109/TMECH.2020.2978529.
- [34] Connor J Boss and Vaibhav Srivastava. A high-gain observer approach to robust trajectory estimation and tracking for a multi-rotor uav. *arXiv preprint arXiv:2103.13429*, 2021. doi: 10.48550/arXiv.2103.13429.
- [35] Joonho Lee, Joochwan Seo, and Jongeun Choi. Output feedback control design using extended high-gain observers and dynamic inversion with projection for a small scaled helicopter. *Automatica*, 133:109883, 2021. doi: 10.1016/j.automatica.2021.109883.
- [36] Xing Fang, Aiguo Wu, Yujia Shang, and Na Dong. Robust control of small-scale unmanned helicopter with matched and mismatched disturbances. *Journal of the Franklin Institute*, 353(18):4803–4820, 2016. doi: 10.1016/j.jfranklin.2016.09.016.
- [37] Robert Mahony, Vijay Kumar, and Peter Corke. Multirotor aerial vehicles: Modeling, estimation, and control of quadrotor. *IEEE robotics & automation magazine*, 19(3): 20–32, 2012. doi: 10.1109/MRA.2012.2206474.
- [38] Samir Bouabdallah and Roland Siegwart. Full control of a quadrotor. In *2007 IEEE/RSJ international conference on intelligent robots and systems*, pages 153–158. Ieee, 2007. doi: 10.1109/IROS.2007.4399042.
- [39] Samir Bouabdallah and Roland Siegwart. Towards intelligent miniature flying robots. In *Field and Service Robotics: Results of the 5th International Conference*, pages 429–440. Springer, 2006. doi: 10.1007/978-3-540-33453-8_36.
- [40] Simone Martini, Serhat Sönmez, Alessandro Rizzo, Margareta Stefanovic, Matt J Rutherford, and Kimon P Valavanis. Euler-lagrange modeling and control of quadrotor uav with aerodynamic compensation. In *2022 International Conference on Unmanned Aircraft Systems (ICUAS)*, pages 369–377. IEEE, 2022. doi: 10.1109/ICUAS54217.2022.9836215.
- [41] Richard L Wheeden. *Measure and integral: an introduction to real analysis*, volume 308. CRC press, 2015.

- [42] Crazyflie 2.1, 2023. URL <https://store.bitcraze.io/products/crazyflie-2-1>.
- [43] TR Beal. Digital simulation of atmospheric turbulence for dryden and von karman models. *Journal of Guidance, Control, and Dynamics*, 16(1):132–138, 1993. doi: 10.2514/3.11437.
- [44] Jeffrey H Ahrens and Hassan K Khalil. High-gain observers in the presence of measurement noise: A switched-gain approach. *Automatica*, 45(4):936–943, 2009. doi: 10.1016/j.automatica.2008.11.012.
- [45] Ricardo G Sanfelice and Laurent Praly. On the performance of high-gain observers with gain adaptation under measurement noise. *Automatica*, 47(10):2165–2176, 2011. doi: 10.1016/j.automatica.2011.08.002.